Journal of Structural Geology, Vol. 10, No. 4, pp. 323 to 333, 1988
Printed in Great Britain

0191-8141/88 $03.00 + 0.00

R_f/ϕ_f strain analysis using an orientation net

DECLAN G. DE PAOR

Department of Earth and Planetary Sciences, The Johns Hopkins University, Baltimore, MD 21218, U.S.A.

(*Received* 23 *March* 1987; *accepted in revised form* 1 *February* 1988)

Abstract—Since the classical work of Cloos, deformed distributions of elliptical objects such as ooids or pebbles have been recognized as an extremely important category of geological strain marker. However, elliptical objects are not easily analyzed, especially where primary sedimentary fabrics are tectonically imbricated. This paper demonstrates that previously published analytical techniques generally address only specific aspects of deformed ellipse distributions; as research tools, they are like a stereonet with great circles only or small circles only. All of the above methods can be combined with the aid of a new orientation net which is as convenient to use in the field as a standard stereonet. Uniform and imbricate fabrics are evaluated with equal ease and assumptions are subjected to statistical testing.

INTRODUCTION

STRAIN data are critical for the proper balancing of cross-sections and may be vital to the correct interpretation of regional tectonic regimes, yet strain analyses are seldom incorporated in regional structural studies, probably owing to: (i) the difficulty of applying strain theory to real rocks; (ii) the general paucity of 'classical' strain markers such as trilobites; and (iii) a hesitancy on the part of the field geologist to undertake complex calculations of dubious validity.

Ellipsoidal objects (ooids, pebbles, reduction spots, varioles, lapilli, xenoliths, etc.) are one of the most important categories of geological strain marker. Because beds or layers containing populations of ellipsoids are commonplace (e.g. Cloos 1947, Hossack 1968), statistically viable data sets can be collected and sectioned in three mutually perpendicular directions, or elliptical outlines can be traced off non-orthogonal joint surfaces; in either case, combinations of two dimensional measurements may be used to yield three-dimensional strain estimates (Ramsay 1967, Oertel 1970, 1978, Roberts & Siddans 1971, Milton 1980, Gendzill & Stauffer 1981, Owens 1984, De Paor 1986 and work in preparation), from which one may determine the two most important deformation parameters, the strain intensity E and the strain ellipsoid symmetry class k (Flinn 1962, see also Hsu 1966). Distributions of ellipsoidal objects in layered stratigraphy record strain variations in space and time (Cloos 1947); maps of such variations are much more useful than individual numerical values. Usually, only the irrotational component of deformation is measurable at any point in space, but the requirement of compatibility among neighboring locations imposes constraints on the relative rotations and translations that may accompany stretch in heterogeneous deformation fields (e.g. Cobbold 1980, Schultz-Ela 1986).

However, whereas the behavior of longitudinal and angular strain markers is relatively simple, equations for ellipse deformation are multivariate and complex. Numerous graphical solutions have been proposed, including the 'R_f/ϕ' method of Ramsay (1967, see Gay 1968, Dunnet 1969, Dunnet & Siddans 1971, Lisle 1977a, 1985), the 'shape factor grid' of Elliott (1970), the 'center-to-center' method of Fry (1979, see Hanna & Fry 1979, Erslev 1987, 1988), and the projection method of Panozzo (1983). A range of algebraic solutions also exists (Oertel 1970, 1978, Matthews *et al.* 1974, Shimamoto & Ikeda 1976, Lisle 1977b, 1979, Robin 1977, Hutton 1979, Pfiffner 1980) (see Appendix) but some cannot deal with primary fabrics and those that do involve unacceptable elements of uncertainty. Practical field geologists are particularly reluctant to become embroiled in technical arguments regarding the relative merits of alternate procedures (e.g. De Paor 1980, 1981a, Siddans 1981, Wheeler 1986). There is a need for amalgamation of published methods incorporating the capability to handle tectonically imbricated fabrics. The solution described here employs a hyperbolic net (De Paor 1981b) that is as easy to use as a standard stereonet and that yields valid results from initially uniform and imbricated fabrics. The net allows simultaneous implementation of many of the methods listed above. It solves the practical problems associated with field implementation of theoretical concepts and leaves the geologist free to concentrate on tectonic implications of the quantitative results.

NOTATION

To describe the shape of an elliptical object independent of its size, one may use either the axial ratio R or the shape factor ε, where

$$\varepsilon = (\ln R)/2 \qquad (1)$$

(see Nadai 1950, Elliott 1970). Long and short axes may be taken in any order, so that $0 < R < \infty$ and $-\infty < \varepsilon < \infty$. Axial orientations are specified by the angle ϕ, here measured positive clockwise from the zero

direction N, which may represent either geographical North or an arbitrary reference direction. The initial, strain and final states are distinguished by subscripts i, s and f, respectively. This is consistent with Elliott (1970); other authors have denoted initial angles by θ, without subscript.

Axial ratios increase multiplicatively under parallel homogeneous strain (Ramsay 1967); for all $\phi = 0$,

$$R_f = R_s \times R_i. \quad (2)$$

In contrast, shape factors increase additively,

$$\varepsilon_f = \varepsilon_s + \varepsilon_i \quad (3)$$

(Nadai 1950, Elliott 1970). Axial ratios are the simplest measures of ellipticity, but shape factors are convenient for certain purposes such as sequential straining and unstraining.

Equations (2) and (3) apply only to ellipses with axes parallel to the principal strain directions. In general, ϕ_i, ϕ_s and ϕ_f differ from zero and from each other, and deformation of an elliptical object is then described by polar co-ordinate pairs which undergo transformations of the form

$$(R_f, \phi_f) = \text{function}\{(R_s, \phi_s), (R_i, \phi_i)\} \quad (4)$$

$$(\varepsilon_f, \phi_f) = \text{function}\{(\varepsilon_s, \phi_s), (\varepsilon_i, \phi_i)\}. \quad (5)$$

The actual functional relationships are somewhat complex and are treated in the Appendix. It is intuitively obvious, however, that the final shape and orientation of an ellipse are independent of its initial size and position; they depend only on initial shape and orientation, along with the shape and orientation of the strain ellipse.

THE HYPERBOLIC NET

The hyperbolic net of De Paor (1981b) comprises two intersecting families of curves (Fig. 1). One family has vertical and horizontal asymptotes and vertices that lie along the diagonals. These track the progressive changes of shape and orientation of ellipses during deformation and therefore they are called *ellipse trajectories*. The second set has symmetric non-orthogonal asymptotes and the vertices lie along the horizontal or vertical axes. These mark equal increments of strain along the trajectories and are called *strain contours*. The two families of curves have appeared under various names in a number of previous publications (Gay 1968, Dunnet 1969, Elliott 1970, Dunnet & Siddans 1971, Lisle 1977a, 1985, Robin 1977, Le Theoff 1979, Wheeler 1984). The difference in Fig. 1 lies in the simple polar co-ordinate plotting scheme employed. Polar co-ordinates are the natural choice as they facilitate operations resembling stereonet procedures.

There are two diametrically opposite directions ϕ and $\phi \pm 180°$ each of which equally represents an ellipse's orientation, just as there are two points on the perimeter of a stereonet representing a plane's strike or a line's trend. This fact affords one the opportunity to treat ellipticity using axial ratios on one side of the net (the 'R-side') and shape factors on the other side (the 'ε-side'). To this end, on the R-side (Fig. 1 top half), ellipse trajectories and strain contours are spaced in regular increments of $\Delta R = 0.2$ (light lines) and $\Delta R = 1.0$ (bold lines) from $R = 1$ at the center of the net up to $R = 5$. To avoid clutter, only $\Delta R = 1.0$ increments are displayed for $R > 5$. On the ε-side (Fig. 1, bottom half), shape factors commence with 0 at the center of the net. Increments of $\Delta\varepsilon = 0.1$ (bold lines) and of $\Delta\varepsilon = 0.05$ (light lines) are marked and are seen to be equally spaced along the axis from the center to the periphery. Diametrically opposite points on the net represent corresponding (R, ϕ) and (ε, ϕ) co-ordinate pairs, so the transformation in equation (1) may be performed graphically by a 180° rotation of a tracing overlay on the net. Note that the net has been arbitrarily terminated at a radius representing axial ratios of $R = 15$. It would have been possible to continue to higher ratios, but the behavior of an ellipse with $R > 15$ differs little from that of a line, so all higher ratios are truncated to $R = 15$. (This procedure is further justified in practice because it is difficult to avoid measurement errors for such high ratios; sometimes one cannot decide whether a single extremely long individual has necked and split in two.) A net of arbitrary range may be generated using a Macintosh computer program available from the author.

PLOTTING PROCEDURE

To plot a point representing an ellipse of axial ratio R_f and orientation ϕ_f (positive clockwise of an arbitrary zero direction N), place a tracing overlay on the net, secure with a central thumb tack, and label the direction N. Rotate the net's R-axis to an angle ϕ_f positive clockwise of N (or, equivalently, rotate the overlay in the opposite direction) (Fig. 2). This is identical to the plotting procedure for the trend of a line on a standard stereonet and is facilitated by 1° (light line) and 10° (bold line) scales in the peripheral ring. Mark a point at distance R_f from the center along the R-axis. Rotate the overlay 180° and plot the point $(R_f, \phi_f \pm 180°)$. The ε_f value corresponding to R_f may now be read off the ε-axis. (This step is not needed immediately, but it is

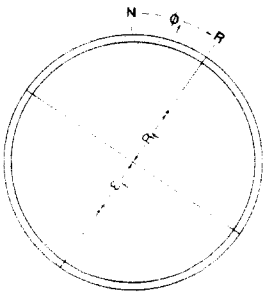

Fig. 2. Plotting procedure for representing an ellipse of orientation ϕ_f and axial ratio R_f or shape factor ε_f. N is an arbitrary reference direction. See text for explanation.

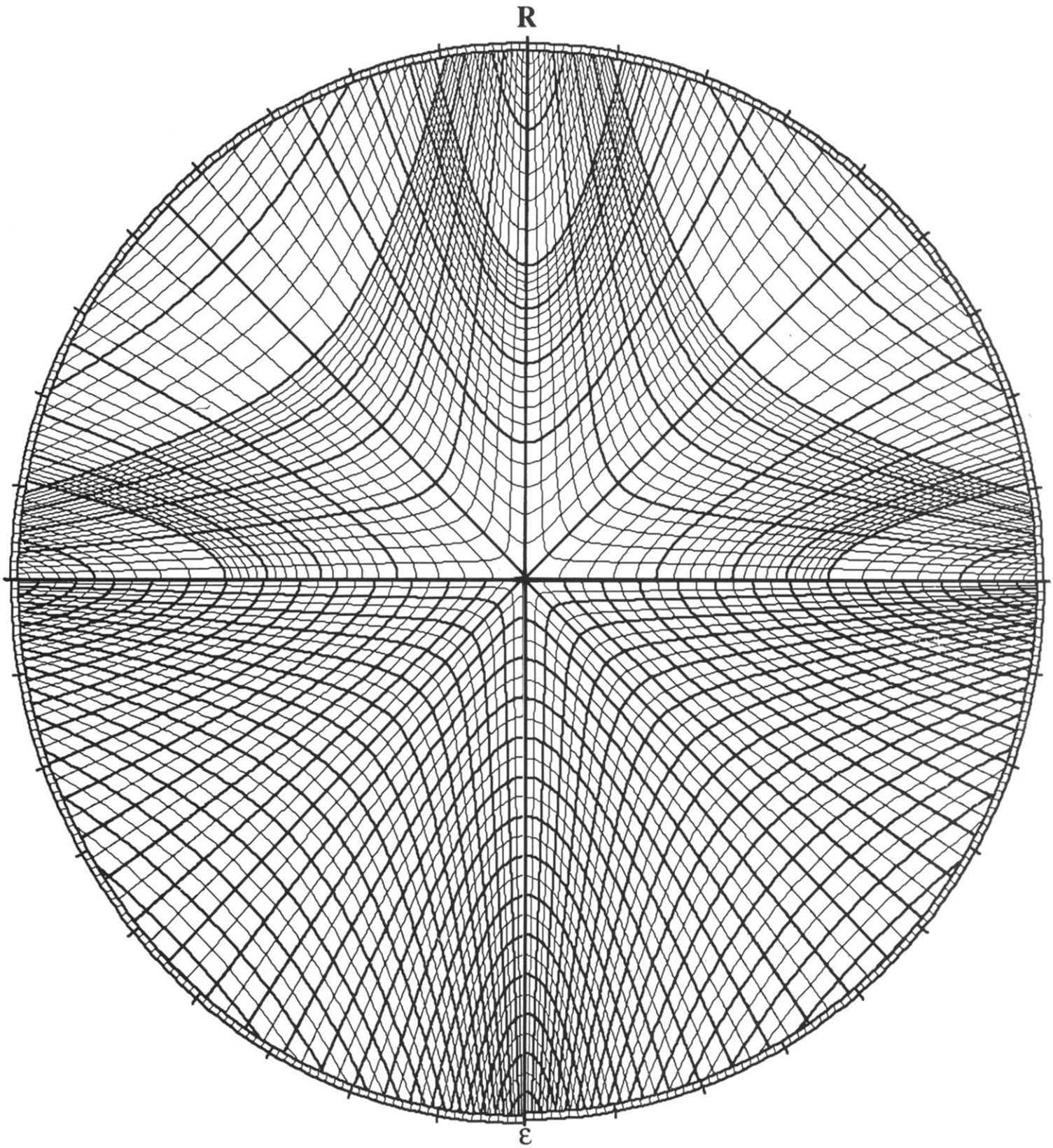

Fig. 1. The hyperbolic net.

useful practice for later; also, by plotting two points per datum, one avoids the mistake of placing part of the distribution on one side of the net and part on the other, if field records of ϕ_f range over 360°.)

STRAIN CALCULATION

Having plotted a complete set of deformed ellipse data, the next step is to estimate the strain recorded by the distribution assuming homogeneous deformation and no primary sedimentary fabric. To do this one simply rotates the net under the tracing overlay until the R-axis divides the population of points on the R-side of the net in half (Fig. 3a). This locates the maximum principal stretch axis orientation, ϕ_s. Previously published techniques use the vector mean ellipse orientation $\bar{\phi}_f$ as an estimate of ϕ_s. However, if the assumption of no primary fabric is valid, then the mean, mode and median of the deformed distribution coincide and the median is the easiest to locate. If there is no gap between orientations of ellipses plotted on the R-side and the ε-side of the net, then no unique median line will be located; this normally implies that the distribution is undeformed.

Without moving the R-axis from its median position, find the strain contour that also divides the population in half (Fig. 3b). It intersects the R-axis at a distance R_s from the origin. By comparison with Dunnet (1969), it is clear that the strain contours represent 50%-of-data curves for successive increments of strain. The above procedure rapidly identifies the particular 50%-of-data curve that fits the deformation state under consideration.

EVALUATION OF RESULTS

The validity of the (R_s, ϕ_s) value obtained above is dependent on the assumptions that the ellipses deformed homogeneously with each other and with their matrix, and that they did not possess a primary sedimentary fabric. Before proceeding to apply two tests of these assumptions, isogons must be constructed for use in the validation procedure.

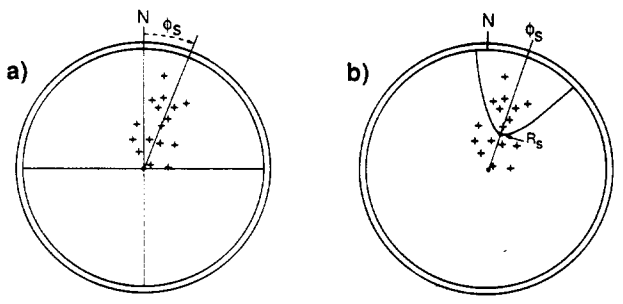

Fig. 3. Strain calculation. (a) After plotting all R_f/ϕ_f data, rotate the net until the R-axis divides the data in half. (b) With the R-axis fixed, find the strain contour which also divides the data in half. Its vertex is at (R_s, ϕ_s).

Isogon construction

Isogons, lines joining points of equal angle, were invented independently by Agterberg (1961) and Elliott (1965) and were applied to dip variations in folds by Ramsay (1967). Here, they are used to identify loci of ellipses with various shapes but identical initial orientation. Such loci were labelled 'θ-curves' by Lisle (1977a, b). Because isogons play a central role in the analysis of deformed ellipse distributions, a locus will be generated from first principles, then a rapid construction will be presented.

For simplicity of notation, but without loss of generality, assume that the arbitrary reference line N is the principal stretch axis as determined in the strain calculation section above (i.e. $\phi_s = 0$). To construct an isogon for the initial orientation ϕ_i, mark N on a tracing overlay, align it with the net axis, and draw a radius across the ε-side of the net at any chosen angle ϕ_i to the principal direction (Fig. 4a). Move every point an equal distance ε_s along the strain trajectories. Then repeat the procedure for a line perpendicular to the first. The outcome is a hyperbola-shaped curve (Fig. 4b). Call the axial intersection point $(R_s, 0)$ and the curve's vertex (R_m, ϕ_m). Strictly, the net's axis divides the curve into separate isogons for the initial angles ϕ_i and $\phi_i \pm 90°$. However, in this paper, R is not restricted to ratios greater than unity, so an ellipse (R, ϕ) is equivalent to $(1/R, \phi \pm 90°)$.

To examine the form of the isogons further, rotate the net until the isogon vertex m lies along the net axis (if ϕ_i happens to be 45° no rotation is required) and note that the ϕ-isogon for a strain of $(R_s, 0)$ is identical to the strain contour ('50%-of-data curve') passing through (R_m, ϕ_m) (Fig. 4c). Expressed another way, each strain contour represents a set of isogons, one for each possible strain ellipse that plots somewhere on it (Fig. 4d). For the strain ellipse that plots at the vertex, it is the 45° isogon (c.f. Lisle 1977a). It follows that isogons for arbitrary values of ϕ_i can be constructed simply by rotating the net until a suitable strain contour passes obliquely through (R_s, ϕ_s). The procedure is analogous to the construction of an inclined stereonet by rotating an equatorial net until each great circle in turn passes through the inclined axis. For a given value of (R_s, ϕ_s), the ϕ value represented by an isogon is determined by rotating the R-axis into the ϕ_s direction and tracing the isogon to its asymptote (∞, ϕ_i), or $(15, \phi_i)$ in practice. Because an infinitely elliptical ellipse is analogous to a line, ϕ_i is determined by Sorby's equation,

$$\tan \phi_i = R_s \tan \phi_f. \quad (6)$$

Sometimes instead of finding ϕ_i for a given isogon, it is necessary to draw the isogon for a given value of ϕ_i. To do this, one first determines ϕ_f from equation (6), and marks a point (∞, ϕ_f) on the periphery of the net. Then by rotating the net until a strain contour asymptotic to (∞, ϕ_f) passes through R_s, the desired curve may be traced. This procedure is analogous to fitting a great circle through an inclined axis at a particular strike angle.

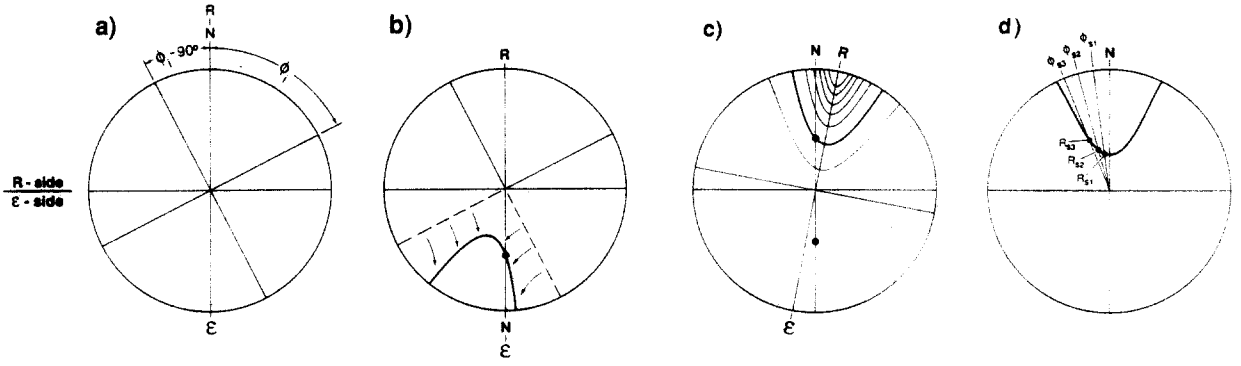

Fig. 4. Derivation of isogons from first principles. (a) A pair of perpendicular radii are drawn on the net. (b) All points on the ε-side are displaced along ellipse trajectories through a certain number of strain contour increments. (c) Net is rotated until the isogon is symmetric about the R-axis. Note that it lies along a strain contour. (d) A single strain contour is interpreted as an isogon of different ϕ_i value for each strain $(R_{s1}, \phi_{s1}), (R_{s2}, \phi_{s2}), (R_{s3}, \phi_{s3})$, etc., that plots along its length.

First test: (R_s, ϕ_s) scatter diagram

To test the assumption of strain homogeneity note that, ideally, every isogon that divides the population in half should pass through (R_s, ϕ_s). Therefore, construct isogons by rotating the net into an arbitrary orientation and finding the strain contour that divides the population in half (Fig. 5). Mark the point of intersection with each previously drawn isogon (points of glancing intersection may be omitted at the user's discretion as they may vary within the thickness of a pencil). Every isogon–isogon intersection is an (R_s, ϕ_s) estimate and the tightness of the cluster of estimates is a measure of the validity of the initial result, which may be thought of as representing the special case of the 0° and 45° isogon intersection. This procedure is analogous to the construction of a 'β-diagram' of great circle intersections on the stereonet (Ramsay 1967, p. 12). If data fail this test, the strain estimate is invalidated.

Second test: primary fabric test

Following Lisle (1977a, b) and Robin (1977), a quantitative measure of the initial orientation distribution is now applied to data passing the test of homogeneity in order to detect any initial sedimentary fabric (Fig. 6).

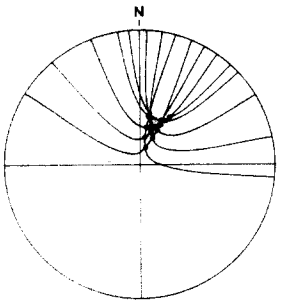

Fig. 5. R_s/ϕ_s scatter diagram to test the assumption of strain homogeneity. With the net axis rotated to an arbitrary orientation, the strain contour that divides the population in half is traced. After several repetitions of the construction, points of intersection of all traced lines are marked, forming a cluster of strain estimates. The tightness of the cluster is an indication of the validity of the strain estimate.

On a new overlay, the centroid of the (R_s, ϕ_s) scatter is chosen as the best strain estimate, then a set of regularly spaced isogons (say 10° or 22.5° apart) are constructed with the aid of Sorby's formula, equation (6) above. This time, all isogons are required to pass through (R_s, ϕ_s) even if they do not divide the population in half. The sectors between each pair of adjacent isogons are expected to contain equal subdivisions of the population for a perfectly uniform initial distribution. Observed sub-populations are compared with those expected using standard χ^2 statistics. Failure of the test may be due to different causes (see Discussion), but primary fabrics are recognized by point concentrations strung out along a specific isogon that was initially parallel or imbricated to bedding (the 'banana' shapes of Elliott 1970 and the 'retort' shapes of Lisle 1985).

Third test: initial shape test

Isogons are loci of equal initial orientation. The equivalent loci of initial shape are termed initial shape contours and are constructed from first principles as follows. First, draw a central circle of arbitrary radius on an overlay (Fig. 7a). Move every point on the ε-side in equal increments $\Delta\varepsilon$ along the ellipse trajectories until any desired strain ε_s has been imposed (note that points perpendicular to the ε-axis are displaced inward, through the center, then out along the axis, representing

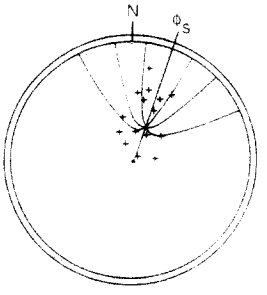

Fig. 6. Test for a primary fabric, after Lisle (1977) and Robin (1977). Isogons representing ϕ_i = 0, 22.5, 45 and 66.5° are constructed through (R_s, ϕ_s) as explained in the text. The numbers of points observed between adjacent isogons are counted and compared with the expected division into equal sub-populations.

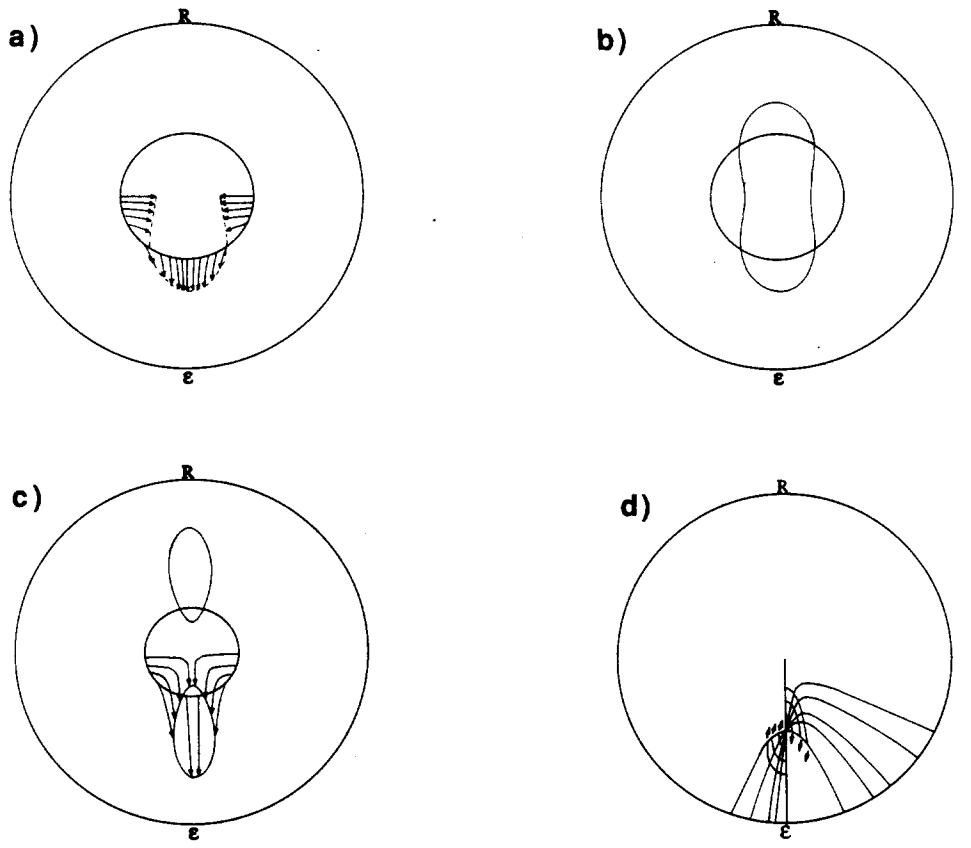

Fig. 7. Construction of initial shape contours from first principles. (a) A central circle is drawn on an overlay. On the ε-side of the net, each point on its perimeter is moved along the ellipse trajectories through an equal number of increments ε_s. (b) Repetition of this construction after 180° rotation of the overlay. (c) Same construction as (b), but for the case $\varepsilon_s > \varepsilon_i$. (d) Rapid construction of nested initial shape contours: upon sequential arbitrary rotations of the net, ε_i increments are set off along the strain contour that passes through $(\varepsilon_s, 0)$.

the behavior of ellipses which contract along their long axis, pass through the circular state, then flip axes). Optionally, rotate the net 180° and repeat (Fig. 7b). The procedure is analogous to the construction of an inclined small circle on an equatorial stereonet by rotation of a vertical small circle. On the hyperbolic net, however, the outcome is a guitar-shaped curve for $R_s < R_i$, changing to a pair of onion-shaped loops when $R_s > R_i$ (Fig. 7c). Varying R_i generates a nested set of initial shape contours converging on (R_s, ϕ_s). A critical observation may now be made on the ε-side of the net. By rotating the net axis until an arbitrary isogon passes through (ε_s, ϕ_s) one may demonstrate that equal increments ε_i are subtended by the isogon's two intersections with each ε_i-contour (the initial shape contour is analogous to a cone of 'centre' ε_s and 'semi-apical angle' ε_i on a standard stereonet). Consequently, a set of initial shape contours may be rapidly constructed as follows: set off any number of $\Delta\varepsilon_i$ increments along the ε-axis, to either side of ε_s (Fig. 7d; the value of $\Delta\varepsilon_i$ may be chosen by converting a desired interval ΔR_i). Then rotate the net a little and set off the same increments along the isogon that passes through $(\varepsilon_s, 0)$. Repeat until a nested set of initial shape contours has been generated. This procedure is analogous to the construction of nested cones on a standard stereonet by setting off the semi-apical angles as a pitch along every great circle that passes through the axis. In all of the above analogies, isogons are equivalent to great circles, initial shape contours to small circles.

By constructing initial shape contours as described above, it is possible to test the uniformity of R_i values as initially proposed by Dunnet (1969). If initial axial ratios were close to a mean value R_i, or always less than a cut-off value R_i-max, then the distribution of (R_f, ϕ_f) data should cluster around, or inside, the corresponding R_i-contour. In practice, it is found that points rarely behave as predicted. R_f/ϕ_f plots often show no relation between data and superimposed contours, implying a random rather than Gaussian distribution of R_i. R_i-contouring is a useful way to obtain initial shape information which may be relevant to sedimentological studies, without actually moving all data along strain trajectories, but the test is of little practical use in evaluating a strain estimate.

PRIMARY FABRICS

If a distribution is not initially uniform, but instead shows a preferred alignment of long axes (e.g. Dunnet & Siddans 1971, Boulter 1976, Holst 1982), its deformed equivalent fails the χ^2 test and the (R_s, ϕ_s) estimate

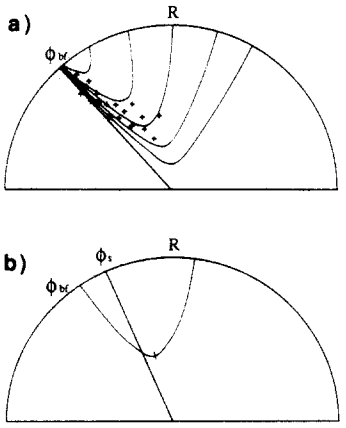

Fig. 8. Strain analysis of a distribution with a primary fabric. (a) R_f/ϕ_f data and final bedding trace ϕ_{bf} are plotted and the median isogon asymptotic to ϕ_{bf} is found. (b) A line drawn in the ϕ_s direction intersects the median isogon in R_s.

obtained above must be abandoned. The following alternative procedure works if the distribution was initially symmetric about a mean direction such as the trace of bedding (Fig. 8). Beginning with the original overlay containing all (R_f, ϕ_f) data plotted relative to an arbitrary reference direction N, add the point (∞, ϕ_{bf}), where ϕ_{bf} is the orientation of bedding after deformation. Rotate the net until each strain contour in turn becomes asymptotic to ϕ_{bf} and examine how it divides the distribution. By successive over- and underestimates, find the isogon that divides the distribution in half. This is the median isogon (thus far, the procedure is analogous to finding a best fit great circle of designated strike ϕ_{bf}). Any point on the median isogon may represent (R_s, ϕ_s). Given an independent estimate of the ϕ_s direction from a mineral elongation or foliation trace (both approximations at best), R_s may be found at the intersection of the median isogon with the ϕ_s direction. Failing that, the range of reasonable (R_s, ϕ_s) values may be bounded by considering the acceptability of R_i values that result from a choice of R_s. Even if one is unable to estimate the range of acceptable R_i values from a knowledge of the undeformed sediment, the state of preservation of pebbles limits the possibilities for R_s. At the very least, the median isogon yields a minimum R_s at its vertex and a range of ϕ_s bounded by the asymptotes.

If an initial line of symmetry ϕ_{bf} is not visible, or if the primary fabric was imbricated oblique to bedding, a median isogon may nevertheless be fitted by trial and error. If all else fails, it is still possible to unstrain data iteratively using the trajectories on the ε-side of the net, and assuming various values of ϕ_s in turn. The iteration is continued until the majority of ε_i values go through minima at the vertices of their ellipse trajectories and begin to increase axial ratio again.

EFFECTS OF VISCOSITY CONTRAST AND NON-COAXIAL DEFORMATION

Lisle (1985) presented a set of isogons for analysis of objects whose viscosity is greater than that of their host rock. Similar isogon sets could be constructed on the hyperbolic net, but this procedure is not recommended, as it is based on the unreasonable assumptions that, in three dimensions, one axis of each object's triaxial ellipsoid is perpendicular to the plane of inspection, and that the plane of inspection is always a principal plane. If these assumptions are dropped, then the material sections of ellipsoidal objects seen in any slice through the rock will not be the same throughout deformation (De Paor 1981a,b). The shapes of final elliptical sections will depend on the lengths and orientations of all ellipsoid axes, all strain axes and the viscosity contrast. Freeman (1985) discovered the important fact that rigid ellipsoids develop a prolate fabric even when deformed in plane strain, but the effect of strain on relatively different viscous objects, as seen in sectional fabrics, has not yet been calculated.

It is now generally accepted that fabric symmetry of deformed ellipses is independent of strain path when there is no viscosity contrast between objects and their matrix (Le Theoff 1979, De Paor 1980, 1981a,b, Wheeler 1984, Lisle 1985). An abstract by Cobbold & Gapais (1983) referred to in Choukroune *et al.* (1987, fig. 2h) suggests that asymmetric nested R_i-contours result from non-coaxial strain of objects that are more viscous than their matrix, although the effect is barely detectable ($<10°$ offset even for strains as high as $R_s = 20$ and viscosity contrasts of $V = 10$). Until more data are available it is not possible to tell whether this conclusion is based on the dubious assumption that all ellipsoids have one axis perpendicular to the principal plane of inspection.

DISCUSSION AND CONCLUSIONS

The analysis of deformed ellipse distributions need not be any more difficult than the manipulation of orientation data on a stereonet. Initial shape contours are analogous to small circles, isogons to great circles. Before deformation, these form concentric circles and radiating straight lines, respectively, just as on a polar stereonet. The effect of deformation is analogous to the rotation of such a net from a polar to an inclined projection. Therefore the fitting of 'onion curves' (Dunnet 1969) is analogous to using an inclined stereonet with small circles but no great circles, while the 'θ-curve' technique of Lisle (1977a) represents the opposite, a net of great circles without small ones. Because different criteria are used to fit 'small' and 'great' circles, comparisons of results show considerable variation (Hanna & Fry 1979, Seymour & Boulter 1979, Paterson 1983, Borradaile 1984, Babaie 1986). Robin's (1977) and Lisle's (1985) approach is a significant advance in that the analogies of great and small circles are used together, but the nets are Cartesian, not polar. The hyperbolic net presented here incorporates all of the plots cited above on its R-side, along with the classical shape factor grid of Elliott (1970, see also Tobisch *et al.* 1977, Wheeler 1984) on the ε-side. Elliott's method has proven less popular

than Dunnet's (but see Holst 1982), probably because of its double polar angle convention and its reliance on a more obscure mathematical derivation based on hyperbolic sines and cosines of natural logarithms, and because of the availability of computer programs for R_f/ϕ analysis by Dunnet & Siddans (1971) and Peach & Lisle (1979). On the hyperbolic net, conversion from axial ratios to shape factors and vice versa is performed by a simple 180° rotation of the overlay.

As an alternative to graphical methods, there exist a set of mathematical techniques involving averages of ellipse or ellipsoid shapes (Oertel 1970, 1978, Matthews *et al.* 1974, Shimamoto & Ikeda 1976, Lisle 1977b, Robin 1977, Miller & Oertel 1979, Pfiffner 1980, Bell 1981, Wheeler 1986, 1987). Techniques that take account of axial ratios only may give a valid approximate strain ratio when fluctuations in orientation are extremely low (Hutton 1979). Of those that take account of ellipse orientations in addition to axial ratios, Robin's method is by far the easiest to use in the field in this author's experience. Some mathematical methods yield rapid results but are unable to detect or deal with primary sedimentary fabrics. Others are theoretically suspect; for example, Wheeler (1986) has shown that Shimamoto & Ikeda's (1976) method is unstable, and the complex analysis presented in Wheeler (1987) is based on the invalid assumption that primary sedimentary fabrics can be modelled by applying a 'virtual' strain to a random fabric. Finally, it must be emphasized that Robin's (1977), Fry's (1979), Panozzo's (1983) and Erslev's (1988) methods are the only ones that adequately deal with non-elliptical initial shapes, or with shapes that become non-elliptical during strain by pressure solution (Mosher 1980, 1981, Onasch 1984). Markers may more closely approximate sub-ellipses or super-ellipses (Fig. 9), given by

$$x^n + y^n = 1, \qquad (7)$$

where $n > 2$ or $n < 2$, respectively (these shapes approximate towards diamonds and television screen shapes; c.f. Lisle 1981). During strain, their axes rotate, respectively, slower or faster than the equivalent ellipse axis ($n = 2$). It is clearly important, therefore, to assess the symmetry of a distribution about all isogons, not only those for $\phi_i = 0°$ and 45°.

None of the techniques discussed in this paper can deal with objects possessing significantly greater viscosity than their matrix, because there is no simple way to describe the resultant heterogeneous strain field. There is no point in devising solutions that require the assumption that all ellipsoids have an axis perpendicular to the plane of inspection.

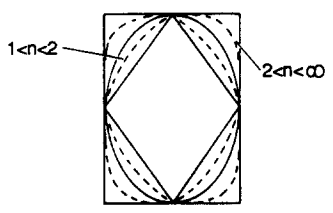

Fig. 9. Illustration of the shapes of sub-ellipses and super-ellipses, see equation (7).

In conclusion, it would seem advisable that the practical geologist should go to the field equipped to carry out (a) Fry analysis or (b) the Robin technique (1977), on deformed objects which have undergone pressure solution or which depart from an elliptical outline, and (c) hyperbolic net analysis of ellipse distributions which may have had a primary fabric. These three techniques cover most eventualities and results can later be transformed into traditional Cartesian R_f/ϕ plots for the sake of familiarity. The stereonet methods described here are not difficult to master; with practice, they permit strain analysis of 50 ellipses per section in about 15 min. What matters in the end is not the calculation of R_s to the third decimal place, but rather whether the three-dimensional deformation state represents contractional, extensional or wrench movements in the crust, whether it departs significantly from plane strain, and whether it can be factored into tectonically meaningful components. To that end, a simple method of reconstructing the three-dimensional strain state from two-dimensional data will be presented in a forthcoming paper.

Acknowledgements—This work was presented in a number of workshops and short courses in Europe and North America. Sue Treagus, Carol Simpson and Richard Lisle provided helpful reviews.

REFERENCES

Agterberg, F. P. 1961. Tectonics of the crystalline basement of the Dolomites in Northern Italy. *Geol. Ultraiect* **8**, 1–232.
Babaie, H. A. 1986. A comparison of two-dimensional strain analysis methods using elliptical grains. *J. Struct. Geol.* **8**, 585–588.
Bell, A. M. 1981. Strain factorization from lapilli tuff, English Lake District, *J. geol. Soc. Lond.* **138**, 463–474.
Borradaile, G. J. 1984. Strain analysis of passive elliptical markers: success of de-straining methods. *J. Struct. Geol.* **6**, 433–437.
Choukroune, P., Gapais, D. & Merle, O. 1987. Shear criteria and structural symmetry. *J. Struct. Geol.* **9**, 525–530.
Cloos, E. 1947. Oolite deformation in the South Mountain Fold, Maryland. *Bull. geol. Soc. Am.* **58**, 843–918.
Cobbold, P. R. 1980. Compatibility of two-dimensional strains and rotations along strain trajectories. *J. Struct. Geol.* **2**, 379–382.
Cobbold, P. R. & Gapais, D. 1983. Pure shear and simple shear of particle matrix systems with viscosity contrasts. *Terra Cognita* **3**, 247 (abstract).
De Paor, D. G. 1980. Some limitations of the R_f/ϕ technique of strain analysis. *Tectonophysics* **64**, T29–T31.
De Paor, D. G. 1981a. Elliptical markers and non-coaxial strain increments—Discussion. *Tectonophysics* **75**, 335–340.
De Paor, D. G. 1981b. Geological Strain Analysis. Unpublished Ph.D. thesis, National University of Ireland.
De Paor, D. G. 1986. Orthographic analysis of geological structures—II. Practical applications. *J. Struct. Geol.* **8**, 87–100.
Dunnet, D. 1969. A technique of finite strain analysis using elliptical particles. *Tectonophysics* **7**, 117–136.
Dunnet, D. & Siddans, A. W. B. 1971. Non-random sedimentary fabrics and their modification by strain. *Tectonophysics* **12**, 307–325.
Elliott, D. 1965. The quantitative mapping of directional minor structures. *J. Geol.* **73**, 865–880.
Elliott, D. 1970. Determination of finite strain and initial shape from deformed elliptical objects. *Bull. geol. Soc. Am.* **81**, 2221–2236.
Erslev, E. A. 1987. Normalized center to center strain analysis. *Geol. Soc. Am. Abs. w. Prog.* **19**, 656.
Erslev, E. A. 1988. Normalized center to center strain analysis of packed aggregates. *J. Struct. Geol.* **10**, 201–209.
Flinn, D. 1962. On folding during three-dimensional progressive deformation. *Q. Jl. geol. Soc. Lond.* **118**, 385–428.

Freeman, B. 1985. The motion of rigid ellipsoidal particles in slow flows. *Tectonophysics* **113**, 163–183.
Fry, N. 1979. Random point distributions and strain measurement in rocks. *Tectonophysics* **60**, 89–105.
Gay, N. C. 1968. Pure shear and simple shear deformation of inhomogeneous viscous fluids. 2. The determination of the total finite strain in a rock from objects such as deformed pebbles. *Tectonophysics* **5**, 295–302.
Gendzwill, D. J. & Stauffer, M. R. 1981. Analysis of triaxial ellipsoids: their shapes, plane sections, and plane projections. *Math. Geol.* **13**, 135–152.
Hanna, S. S. & Fry, 1979. A comparison of methods of strain determination in rocks from southwest Dyfed (Pembrokeshire) and adjacent areas. *J. Struct. Geol.* **1**, 155–162.
Holst, T. B. 1982. The role of initial fabric on strain determination from deformed ellipsoidal objects. *Tectonophysics* **82**, 329–350.
Hossack, J. R. 1968. Pebble deformation and thrusting in the Bygdin area (southern Norway). *Tectonophysics* **5**, 315–339.
Hsu, T. C. 1966. The characteristics of coaxial and non-coaxial strain paths. *J. Strain Anal.* **1**, 216–222.
Hutton, D. H. W. 1979. The strain history of a Dalradian slide: using pebbles with low fluctuation in axis orientation. *Tectonophysics* **55**, 261–273.
Le Theoff, B. 1979. Noncoaxial deformation of elliptical particles. *Tectonophysics* **53**, T7–T13.
Lisle, R. J. 1977a. Clastic grain shape and orientation in relation to cleavage from the Aberystwyth Grits, Wales. *Tectonophysics* **39**, 381–395.
Lisle, R. J. 1977b. Estimation of the tectonic strain ratio from the mean shape of deformed elliptical markers. *Tectonophysics* **56**, 140–144.
Lisle, R. J. 1979. Strain analysis using deformed pebbles: The influence of initial pebble shape. *Tectonophysics* **60**, 263–277.
Lisle, R. J. 1981. The exact shape of deformed pebbles. *J. Struct. Geol.* **3**, 189 (abstract).
Lisle, R. J. 1985. *Geological Strain Analysis: A Manual for the R_f/ϕ Technique*. Pergamon, Oxford.
Matthews, P. E., Bond, R. A. B. & Van den Berg, J. J. 1974. An algebraic method of strain analysis using elliptical markers. *Tectonophysics* **24**, 31–67.
Miller, D. & Oertel, G. 1979. Strain determination from the measurement of pebble shapes: a modification. *Tectonophysics* **55**, T11–T13.
Milton, N. J. 1980. Determination of the strain ellipsoid from measurements on any three sections. *Tectonophysics* **64**, T19–T27.
Mosher, S. 1980. Pressure solution deformation of conglomerates in shear zones, Narragansett Basin, Rhode Island. *J. Struct. Geol.* **2**, 219–225.
Mosher, S. 1981. Pressure solution deformation of the Purgatory Conglomerate from Rhode Island. *J. Geol.* **89**, 35–55.
Nadai, A. 1950. *Theory of Flow and Fracture of Solids*. McGraw-Hill, New York.
Oertel, G. 1970. Deformation of a slaty lapillar tuff in the Lake District, England. *Bull. geol. Soc. Am.* **81**, 1173–1187.
Oertel, G. 1978. Strain determination from the measurement of pebble shapes. *Tectonophysics* **50**, T1–T8.
Onasch, C. M. 1984. Application of the R_f/ϕ technique to elliptical markers deformed by pressure solution. *Tectonophysics* **110**, 157–165.
Owens, W. H. 1984. The calculation of a best-fit ellipsoid from elliptical sections on arbitrarily oriented planes. *J. Struct. Geol.* **5**, 611–618.
Panozzo, R. 1983. Two-dimensional analysis of shape fabric using projections of digitized lines in a plane. *Tectonophysics* **95**, 279–294.
Paterson, S. R. 1983. A comparison of methods used in measuring finite strains from ellipsoidal objects. *J. Struct. Geol.* **5**, 611–618.
Peach, C. J. & Lisle, R. J. 1979. A FORTRAN IV program for the analysis of tectonic strain using deformed elliptical markers. *Comp. & Geosci.* **5**, 325–334.
Pfiffner, O. A. 1980. Strain analysis in folds (Infrahelvetic Complex, Central Alps). *Tectonophysics* **61**, 337–362.
Ramsay, J. G. 1967. *Folding and Fracturing of Rocks*. McGraw-Hill, New York.
Roberts, B. & Siddans, A. W. B. 1971. Fabric studies in the Llwyd Mawr ignimbrite, Caernarvonshire, North Wales. *Tectonophysics* **12**, 283–306.
Robin, P.-Y. F. 1977. Determination of geologic strain using randomly oriented strain markers of any shape. *Tectonophysics* **42**, T7–T16.
Schultz-Ela, D. D. 1986. Strain models for the evolution of a northern Minnesota greenstone belt. *Geol. Soc. Am. Abs. w. Prog.* **18**, 741.
Shimamoto, T. & Ikeda, Y. 1976. A simple algebraic method for strain estimation from deformed ellipsoidal objects. *Tectonophysics* **36**, 315–317.
Siddans, A. W. B. 1981. Some limitations of the R_f/ϕ technique of strain analysis—discussion and reply. *Tectonophysics* **72**, 155–158.
Seymour, D. B. & Boulter, C. A. 1979. Tests of computerized strain analysis methods by the analysis of simulated deformation of natural unstrained sedimentary fabrics. *Tectonophysics* **58**, 221–235.
Tobisch, O. T., Fiske, R. S., Sacks, S. & Tanguchi, D. 1977. Strain in metamorphosed volcanoclastic rocks and its bearing on the evolution of orogenic belts. *Bull. geol. Soc. Am.* **88**, 23–40.
Wheeler, J. 1984. A new plot to display the strain of elliptical markers. *J. Struct. Geol.* **6**, 417–423.
Wheeler, J. 1986. Average properties of ellipsoidal fabrics: implications for two- and three-dimensional methods of strain analysis. *Tectonophysics* **126**, 259–270.
Wheeler, J. 1987. Strain analysis in rocks with pretectonic fabrics. *J. Struct. Geol.* **8**, 887–896.

APPENDIX

DERIVATION OF EQUATIONS

To facilitate readers who may wish to check the validity of practical applications described in the main paper, or to compare results of various methods, the equations governing deformed ellipse distributions are derived here from first principles. If ellipses are represented in Mohr space, using the reciprocal quadratic stretch and reciprocal shear strain parameters (λ', γ') of Nadai (1950), then their transformation under strain follows a simple straight line path. Ellipses of axial ratio R are represented by a common Mohr circle regardless of orientation, but a specific pole to the Mohr circle distinguishes an ellipse of particular orientation ϕ from all other ellipses with the same axial ratio (Fig. A1). If (λ_i', γ_i') are the pole co-ordinates for an initial ellipse, the corresponding final pole co-ordinates (λ_f', γ_f') resulting from imposition of tectonic strain $(\lambda_s', 0)$ are given by Ramsay (1967, p. 93).

$$\lambda_f' = \lambda_s' \lambda_i' \quad \text{(A1)}$$
$$\gamma_f' = \gamma_i' \quad \text{(A2)}$$

(see Fig. A2). These are the fundamental transformations of R_f/ϕ_f strain analysis in the simplest possible format.

The Mohr circle representing an ellipse of axial ratio R intersects the horizontal reference axis at $(R, 0)$ and $(1/R, 0)$. Thus the circle's center (C,0) and radius S are given by

$$C = \frac{R + 1/R}{2} \quad \text{(A3)}$$
$$S = \frac{R - 1/R}{2} \quad \text{(A4)}$$

so that

$$C^2 - S^2 = 1. \quad \text{(A5)}$$

From Fig. A3, the pole co-ordinates may be expressed in terms of C, S and ϕ,

$$\lambda' = C - S \cos 2\phi \quad \text{(A6)}$$
$$\gamma' = S \sin 2\phi. \quad \text{(A7)}$$

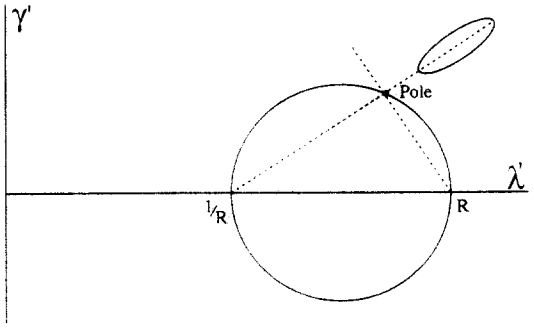

Fig. A1. Mohr circle representing an ellipse of axial ratio R in λ'/γ' space. P is the pole which distinguishes this ellipse from others of equal axial ratio but different orientation.

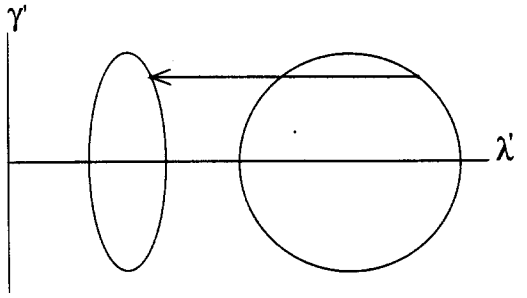

Fig. A2. Transformation of (λ_i', γ_i') pole co-ordinates to (λ_f', γ_f') upon imposition of deformation $(\lambda_i', 0)$ according to equations (A1) and (A2). Note that the set of poles on a common Mohr circle represent an initial shape contour, and that they transform from a circle to an ellipse with a vertical to horizontal axial ratio R_s.

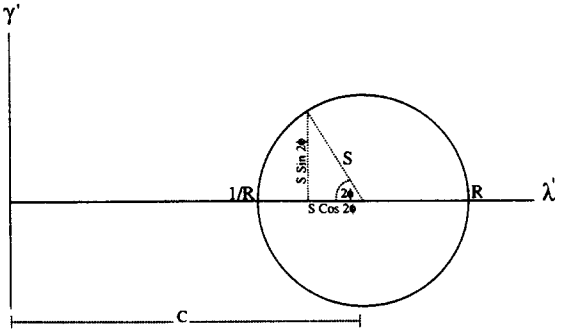

Fig. A3. Explanation of equations (A3)–(A7). See text for details.

Conversely, given the pole co-ordinates (λ', γ'), R and ϕ may be obtained by simultaneous solution of the pair of equations

$$\tan \phi = \gamma'/(R - \lambda') \quad \text{(A8)}$$
$$\cot \phi = \gamma'/(\lambda' - 1/R). \quad \text{(A9)}$$

Equation (A1) may be rewritten using equation (A6) in two ways, with the strain ellipse long axis as reference direction and an axial ratio of R_s, or with the short axis as reference direction and an axial ratio of $1/R_s$. Noting that $R_s = 1/\lambda_s'$,

$$(C_f - S_f \cos 2\phi_f)R_s = C_i - S_i \cos 2\phi_i \quad \text{(A10)}$$
$$(C_f + S_f \cos 2\phi_f)/R_s = C_i + S_i \cos 2\phi_i. \quad \text{(A11)}$$

Adding, and using equations (A3) and (A4) for the strain state,

$$C_fC_s - S_fS_s \cos 2\phi_f = C_i \quad \text{(A12)}$$

or

$$\sec 2\phi_f = \frac{S_fS_s}{C_fC_s - C_i}. \quad \text{(A13)}$$

This equation, which is independent of ϕ_i, is the equation of an initial shape contour. If, following Nadai (1950, equations 3–15), we let S denote $\sinh 2\varepsilon$ and C denote $\cosh 2\varepsilon$, then equation (A12) is analogous to Dunnet's (1969) equation (28).

Dividing equation (A10) by R_s and multiplying (A11) by R_s, then adding, yields

$$C_f = C_iC_s + S_iS_s \cos 2\phi_i \quad \text{(A14)}$$

which is Elliott's (1970) equation (24), whereas subtracting equation (A11) from equation (A10) yields

$$S_f \cos 2\phi_f = C_iS_s + S_iC_s \cos 2\phi_i. \quad \text{(A15)}$$

From equations (A2) and (A7),

$$S_f \sin 2\phi_f = S_i \sin 2\phi_i \quad \text{(A16)}$$

so dividing equations (A15) by (A16) yields

$$\cot 2\phi_f = Ct_iS_s \operatorname{cosec} 2\phi_i + C_s \cot 2\phi_i, \quad \text{(A17)}$$

where Ct denotes $\coth 2\varepsilon$. Equation (A17) is Elliott's (1970) equation (23) as typographically corrected by Tobisch *et al.* (1977). Equations (A14) and (A17) together describe the trajectories of ellipses in terms of initial and strain parameters.

To obtain an expression for the strain contours, set $\phi_i = 45°$ in equations (A14) and (A15),

$$C_f = C_iC_s \quad \text{(A18)}$$
$$S_f \cos 2\phi_f = C_iS_s \quad \text{(A19)}$$

then eliminating C_i yields

$$T_f = T_s \sec 2\phi_f, \quad \text{(A20)}$$

where T denotes $\tanh 2\varepsilon$. For an isogon with vertex (R_m, ϕ_m), from equation (A20),

$$T_f = T_m \sec 2(\phi_f - \phi_m), \quad \text{(A21)}$$

where

$$T_m = T_s \cos 2\phi_m. \quad \text{(A22)}$$

Hence

$$T_f = T_s \sec 2(\phi_f - \phi_m) \cos 2\phi_m. \quad \text{(A23)}$$

To find this isogon's equation in terms of ϕ_i and not ϕ_m, divide equation (A12) by equation (A16),

$$Ct_i = Ct_fC_s \sin 2\phi_i \operatorname{cosec} 2\phi_f - S_s \sin 2\phi_i \cot 2\phi_f \quad \text{(A24)}$$

and then use equation (A17) to eliminate Ct_i,

$$Ct_f = C_s \cos 2\phi_f - \sin 2\phi_f \cot 2\phi_i. \quad \text{(A25)}$$

Finally, one may obtain an exact solution for (R_s, ϕ_s). Assuming an initially uniform distribution, first calculate the average (or median) ellipse orientation, ϕ_m, as an estimate of ϕs. Then equation (A20) may be written in pocket calculator format,

$$R_s = \exp(\operatorname{arctanh}(\overline{\tanh(\ln(R_f) \times \cos 2(\phi_f - \phi))})), \quad \text{(A26)}$$

where the bars denote medians of all stored (R_f, ϕ_f) data. To test the assumption of uniformity, equation (A26) should be solved separately for data on either side of ϕ_m. If the population was initially uniform, it will be symmetric about ϕ_m after deformation, and the two solutions will match. An exact solution is also possible for tectonically imbricated fabrics by first determining the median value of T_m from equation (A21) and then using an independent estimate of ϕ_m in equation (A22) to calculate T_s and hence R_s.